Microfluidic Bulk-Modulus Measurement by a Nanowavelength Longitudinal-Acoustic-Wave Microsensor in the Nonreflective Regime

Yao Lu, Menglun Zhang,[*] Hongxiang Zhang, Yuan Jiang, Hao Zhang, and Wei Pang[†]

State Key Laboratory of Precision Measuring Technology & Instruments, Tianjin University, Tianjin 300072, China

Due to their easy, fast, and noninvasive natures, acoustic wave methods have been widely used in the physical property measurements of liquids, such as shear waves for viscosity and ultrasound for density. We investigate the physical interaction between approximately GHz longitudinal acoustic waves and simple Newtonian fluids in micro- and nanoscales, and report a longitudinal-acoustic-wave microsensor for microfluidic bulk-modulus measurement. We also verify that the microsensor is insensitive to viscosity, in contrast to shear-wave sensors commonly used for viscosity measurements. With its small size and nanometer wavelengths, the microsensor in nonreflective regimes can be integrated into microfluidics and can make fast measurements even under harsh conditions, such as in limited (15∼200 μm) channel spaces and sample volumes (approximately μl). The longitudinal-acoustic-waves measuring theory is demonstrated by the Mason model, a finite element analytical model, and experiments on glycerol-water mixture samples. The microsensor is originally designed for microfluidic use, nevertheless, it can be used under diverse conditions in which miniaturization matters, namely, in biomedical, chemistry, industry, environmental, healthcare, energy applications, and so on.

I. INTRODUCTION

The measurement of liquid physical parameters (density, viscosity, bulk modulus, permittivity, conductivity, etc.) is indispensable in applications ranging from *in vitro* diagnosis and chemosynthesis to genetic engineering in the life sciences and other important fields [1–4]. Miniaturization and high sensitivity are two of the most vital trends associated with measurement systems, making micro- and nanosensors desirable [5,6]. Moreover, the emergence and advancement of microfluidic technology have enabled precise and complex control over tiny volumes of fluids at the micro- and even nanoscales, which also contributes to the miniaturization of liquid phase measurements [7,8]. Briefly, miniaturized sensors and microfluidic technologies have paved the way for highly sensitive and portable measurements. For example, use of micromechanical cantilevers [9], nano-optomechanical disks [10], microelectromechanical resonators [11], and surface acoustic waves [12] are common methods for density, mass, and viscosity measurements and the integrated system including microfluidics and miniaturized sensors has made remarkable progress [13,14].

Among these approaches for liquid phase measurement, the acoustic wave method is noninvasive, passive, gives

fast sample to results, and has been widely used in fluid applications. Different types of acoustic microsensors, including A0/S0 mode Lamb wave sensor [15,16], surface acoustic wave devices [17], thickness-shear-mode sensors [18], quartz crystal microbalance (QCM) [19], and longitudinal film-bulk-acoustic-resonators (FBAR) [20,21], differ in operations, properties, and perspectives. Each type has its specific advantages and disadvantages, and therefore, its particular applications. A common, fast, and efficient method is the use of shear acoustic waves, in which shear force acts on fluids at the solid-liquid interface, causing layers in liquids to produce a shear velocity gradient due to the effect of viscosity. Numerous microsensors based on this principle have been developed, such as the shear-mode thin-film bulk-acoustic-wave sensor [22,23], shear-mode solidly mounted sensor [24–26], QCM [27], shear-surface transverse-acoustic-wave sensor [28], and capacitive micromachined ultrasonic transducer [29]. The resonant frequency of these shear-mode resonant sensors is proportional to the square root of the product of the density and viscosity, according to the principle derived by Kanazawa and Gordon [30].

However, it is worth noting that approximately GHz shear waves can only penetrate a few tens of nanometers in general Newtonian liquids [30], not to the interior of a bulk liquid, because elastic shear motion cannot propagate in fluids [31]. In other words, shear-wave sensors cannot detect the compressional properties of liquids such

*zml@tju.edu.cn
†weipang@tju.edu.cn

as the bulk modulus. On the other hand, longitudinal acoustic waves (LAWs) can propagate effectively in liquids due to the compressional force along the direction of vibration, which lays the fundamental basis for liquid compressional property measurement by longitudinal acoustic waves [32,33]. The distinctive feature of LAWs sensors makes the corresponding measurements completely different from shear-wave sensors. As an important parameter reflecting the compressional properties of liquids, the bulk modulus is closely related to the chemical bond strength between atoms, ions, or molecules at the microscale. It can be used in analyzing human physiological fluids for studying human diseases or tissues [34,35]. Previous studies on the liquid bulk-modulus measurement mainly focused on large-scale hydraulic systems [36,37] and they used bulky and complex sensors. To the authors' knowledge, liquid bulk-modulus measurements on microscales (i.e., microfluidics) are still lacking.

In order to measure the liquid bulk modulus by LAWs in a simple and easy way, two prerequisites have to be met. The first is the nonreflective requirement, which means that no reflective waves coming from exterior liquid environment should be received by LAWs microsensors. Although LAWs propagating in a liquid inevitably suffer from energy loss, the intrinsic resonant frequency of the acoustic wave sensor essentially determines the waves' nonreflective working range in that liquid. For low-frequency LAWs sensors working at MHz or kHz, they require millimeters or even meters to avoid the reflection of acoustic waves. The nonreflective requirement in a microfluidic channel is nontrivial for these sensors. For example, a piezoelectric bulk piezoelectric transducer-based LAW sensor needs an extra wedge reflector to prevent reflection [38]. LAWs sensors with gigahertz resonant frequency (2–20 GHz) can generate nanowavelength acoustic waves in liquids, for example, 75–750 nm wavelengths. Microfluidic [39] and nanofluidic [40] channels have been integrated onto nanowavelength LAWs sensors for liquid property measurements. But these channel heights (e.g., 500 nm) are too small to avoid acoustic wave reflection. The second prerequisite is to use a pure longitudinal mode. Generally, a bulk-acoustic-wave (BAW) sensor excites both types of waves, hence BAW sensors are susceptible to viscosity.

In this paper, we highlight the capacity of nanowavelength LAWs sensors for liquid bulk-modulus measurements in microfluidics with a focus on the nonreflective regime. Theoretical models are introduced to quantify the electrical response of sensors to a sample liquid. Finite element method (FEM) simulation presents the nonreflective measurement results of nanowavelength waves on the microscale. Experimental results are consistent with these models, and the relationship between the key parameters of LAW sensors and liquid bulk modulus are established. From an academic perspective, our work investigates the interaction between nanowavelength acoustic waves and

liquid at the solid-liquid interface. From an application perspective, our work fills the gaps in current liquid bulk-modulus measurements at the microscale and it paves the way to alternative applications in in-field analysis and point-of-care testing, where low sample consumption, fast sample to results, high throughput, and instrument portability are preferable or necessary. For example, the LAWs microsensors introduced in this work can potentially be used for measurements in a portable way: detection of food deterioration and wine quality identification for food applications, water quality monitoring for environmental applications, and disease early diagnosis based on measurements of saliva, urine, sweat, and even blood for medical applications. Together with microfluidic technologies, the LAWs microsensors can realize the above applications on the spot, at home or at an office, instead of going to hospitals, laboratories, and other centralized facilities.

II. MEASUREMENT SYSTEM DESCRIPTION

In this work, the bulk-modulus measuring system is based on the acoustic interaction of LAWs and microfluidics. Figure 1 provides a measurement schematic diagram of the acoustic wave sensor coupled in a microfluidic channel. The microsensor we use in this work excites approximately 2.5-GHz acoustic waves and the corresponding acoustic wavelength is approximately 600 nm in water. The wavelength may vary with different liquids and frequencies (i.e., shorter wavelength at a higher frequency and in a liquid with low acoustic velocity). The microsensor excites longitudinal acoustic waves and it is completely immersed in the liquid where the acoustic waves propagate perpendicular to the surface (z axis) of the device and interact with the liquid. These typical acoustic interactions enable the response of the microsensor to directly reveal the compressional information of various liquids and are practically unaffected by the viscosity of the liquid.
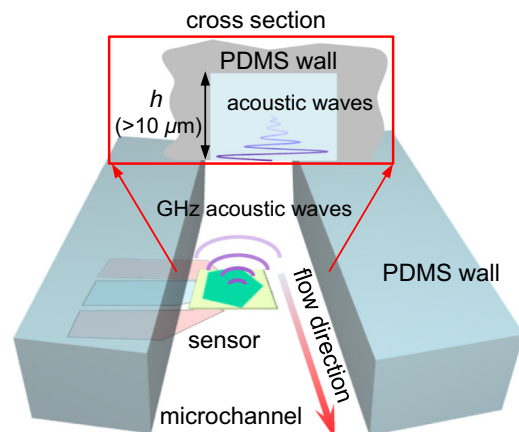

FIG. 1. The schematic diagram of microfluidic bulk-modulus sensing by longitudinal mode microsensor.

We fabricate the approximately 2.5-GHz acoustic microsensors by thin-film fabrication technology [41]. The cross section of the acoustic microsensor is shown in the SEM image in Fig. 2(a). The $SiO_2/Mo/SiO_2/Mo/SiO_2$ thin-film stack is first deposited on the Si substrate by the chemical vapor deposition method, acting as an acoustical Bragg reflector for effective acoustic energy reflection. The layers of Mo and SiO_2 exhibit high and low acoustic impedances, respectively. The thickness of each layer is one-fourth of the acoustic wavelength. Such acoustic microsensors with Bragg reflectors exhibit better mechanical stability and quality factors than do the sensors with air cavities [42] when immersed in liquid environments. The Mo layer with a 200-μm thickness is then sputter deposited and patterned on the Bragg reflector, forming the bottom electrode of the microsensor. Highly *c* axis-oriented AlN thin film (1.1 μm) is sputter deposited as a piezoelectric layer, which transforms electrical energy into mechanical vibrations and vice versa. Another Mo layer with a 200-μm thickness is sputter deposited and patterned, forming the top electrode. One-μm thick SiO_2 is deposited on top of the top electrode to electrically insulate the sensor from the sample liquid, which may be electrically conductive. When the sensor works in air, the top side of the acoustic wave sensor with a solid-air interface creates a large acoustic impedance mismatch to confine acoustic energy in the sensor to reach maximum resonance at its resonant frequency. On the other hand, when the sensor is loaded with liquid on top of the active area, a large portion of acoustic wave energy leaks into the liquid due to a decreased acoustic impedance mismatch compared with that at the solid-air interface, which weakens the resonance remarkably. Nevertheless, part of the wave energy is reflected back into the sensor at the interface.

The polydimethylsiloxane- (PDMS) based microchannel fabricated by soft lithography technology in this work is ten to dozens of microns high and is assembled above the excitation region of the acoustic wave sensor. The height of the microchannel used here could satisfy the nonreflective propagation of a longitudinal wave in liquids,

as discussed in the section on nonreflective measurement (Sec. IV B). After surface decontamination (ultrasonic cleaning with 1:1 mixture of alcohol and deionized (DI) water for 5 min, and then with DI water for 5 min), the microchannel and microsensor are aligned and bonded under a microscope (5X, Nikon). The top view (left) and sectional view (right) micrographs in Fig. 2(b) show an 18-μm high, 150-μm wide microchannel; the active pentagonal area (approximately 10^4 μm^2) of the microsensor features three electrodes (ground-signal-ground) extending outside the PDMS wall for electrical testing. When alternating current power (0.01 mW) is applied to the three pads (Au electrodes) via a probe connected to the network analyzer, the acoustic wave sensor excites GHz longitudinal waves and produces resonance via the inverse piezoelectric effect. Furthermore, the high acoustic velocity (approximately km/s) at the microscale enables the response results to be presented immediately as long as the acoustic wave is changed. The electrical signal of the microsensor can be received through the network analyzer.

III. THEORY AND NUMERICAL MODEL

Based on the interaction between the longitudinal waves and fluids, we can infer that the acoustic impedance of the loaded liquid will determine the amount of reflected acoustic wave energy. Thus, the electrical impedance (Z_e) obtained at the electrical ports of the microsensor, an indicator of acoustic wave transmission and reflection, depends on the matching degree of the acoustic impedance between the microsensor and external loading. Furthermore, the acoustic impedance of liquid is defined as follows [43]:

$$Z = \sqrt{\rho M^*}, \tag{1}$$

where ρ and $M^* = K^* + 4/3G^*$ are density and complex longitudinal-wave modulus, respectively. For simple Newtonian fluids, the longitudinal-wave modulus is determined by bulk modulus (K^*) and shear modulus (G^*) [43,44]. Clearly, the acoustic impedance, which includes compressional information associated with the loaded liquids, can be analyzed by measuring the electrical impedance of the LAWs microsensor. Remarkably, all of these principles are based on the premise that longitudinal acoustic waves can propagate in liquids.

In order to analyze the electrical response of the LAWs microsensor to the liquid, a classical Mason model [45] is used, in which all layers of the sensor are treated as a sequence of transmission lines. Figure 3 shows a one-dimensional acoustic transmission line model with a parallel-liquid stack loaded on the microsensor. All the layers are connected in series according to the structure of the LAWs microsensor. The acoustic impedance of the stacked layers below (Bragg reflector, bottom electrode)
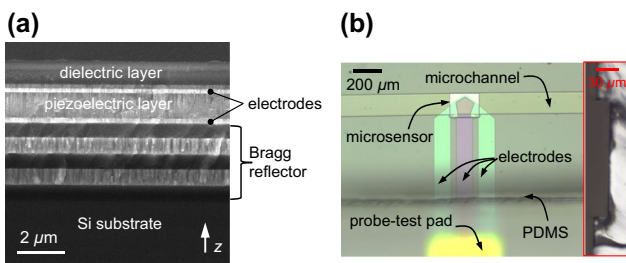
(a)   **(b)**

dielectric layer
piezoelectric layer — electrodes
Bragg reflector
2 μm   Si substrate z

200 μm   microchannel
microsensor
electrodes
probe-test pad   PDMS

FIG. 2. (a) The cross section of microsensor via SEM. (b) The photo of 18-μm height PDMS-based microchannel assembled on the active area of a microsensor and its enlarged view under a microscope.
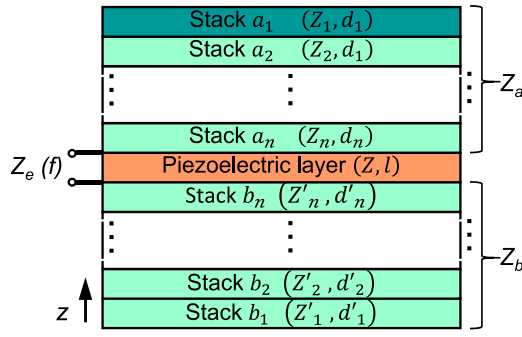
FIG. 3. The transmission line model of the longitudinal mode microsensor with loaded parallel-liquid stack, Z_e is the measured electrical impedance of the microsensor and Z_a, Z_b are the acoustic impedances of other functional stacks above and below the piezoelectric layer, respectively.

and above (top electrode, dielectric layer, and liquid layer) the piezoelectric layer are denoted Z_b and Z_a, respectively. The electrical impedance at both ends of the piezoelectric layer is denoted Z_e. The Mason model uses the acoustic and piezoelectric equations to describe the stress fields in the layer stack and the electrical impedance [45]. These derivations start from fundamental equations [46], shown below by the Newton's second law and Hooke's law

$$\frac{\partial T}{\partial z} = \rho \frac{\partial v}{\partial t}, \frac{\partial T}{\partial t} = c \frac{\partial v}{\partial z}, \tag{2}$$

where T, v, c, and ρ represent the normal stress, acoustic velocity, modulus along the z axis, and density of the solid material, respectively. The acoustic impedance of a stack can be calculated by recursive computations of a transmission line equation [45]

$$Z_{\text{in}} = Z_0 \frac{Z_t \cos\left(\frac{2\pi}{v}f\,\text{d}\right) + j Z_0 \sin\left(\frac{2\pi}{v}fd\right)}{Z_0 \cos\left(\frac{2\pi}{v}fd\right) + j Z_t \sin\left(\frac{2\pi}{v}fd\right)}, \tag{3}$$

in which Z_0 is the characteristic acoustic impedance, v is the acoustic velocity of the material, d is the layer thickness, and Z_t is the terminating impedance. Thus, we can derive that Z_a and Z_b are related to the acoustic impedance and thickness of each layer. The functional equation is simplified as

$$Z_a = g(Z_1, Z_2, \ldots, Z_n; d_1, d_2, \ldots, d_n), \tag{4}$$

$$Z_b = g'(Z'_1, Z'_2, \ldots, Z'_n; d'_1, d'_2, \ldots, d'_n), \tag{5}$$

where Z_i and d_i are the acoustic impedance and thickness of the ith layer, respectively. Moreover, the Z_e of the piezoelectric layer loaded with Z_a and Z_b can be simply

expressed as follows:

$$Z_e = H(Z_a, Z_b, Z, f, l), \tag{6}$$

where Z, f, and l represent the acoustic impedance, resonant frequency, and thickness of the piezoelectric layer, respectively. Obviously, the measured electrical impedance changes with the abovementioned acoustic impedance Z_a, which is directly dependent on the acoustic impedance (Z_1) of the loading liquid sample. With respect to the propagation of acoustic waves, the solid-liquid interface has a smaller acoustic impedance mismatch than does air, making most of the acoustic energy leak out of the LAWs microsensor. The amount of leaked energy depends on the acoustic impedance of the loading liquid. Since the shear modulus of simple Newtonian fluids is a purely imaginary number [47], the longitudinal-wave modulus of the liquid subjected to a bulk force is described as

$$M^* = K' + i\omega \left(\mu_B + \frac{4}{3}\mu\right), \tag{7}$$

where K', $\omega = 2\pi f$, μ_B, and μ are the real part of bulk modulus, angular frequency, bulk viscosity, and shear viscosity, respectively. Thus, Eq. (1) can be further reduced as follows:

$$Z_{\text{liquid}} = Z_{\text{real}} \left[1 + i\frac{\omega}{K'} \left(\mu_B + \frac{4}{3}\mu\right)\right]^{1/2}, \tag{8}$$

$$Z_{\text{real}} = \sqrt{\rho K'}. \tag{9}$$

We can derive from Eqs. (6) and (8) that the electrical impedance directly changes with the bulk modulus and viscosity, whereas the imaginary part of the acoustic impedance of the liquid has very little effect on the electrical impedance. As exemplified by glycerol-water mixtures, viscosity changes dramatically [48] with different mixing concentrations, but the acoustic impedance varies less than 1%. Conclusively, the electrical impedance reflects the bulk modulus of loaded liquid samples, indicating that a LAWs resonator can be employed as a bulk-modulus sensor by probing the changes of electrical impedance, and the microsensor is insensitive to sample viscosity. It should be noted that the measuring principle is most suitable for simple Newtonian fluids, such as glucose, physiological saline, and ionic solutions. For complex or inhomogeneous fluids with viscoelastic properties, such as blood plasma, the relaxation process [44,49] needs to be considered and Eqs. (7)–(9) need to be further modified [47,50]. Therefore, it would be more complex since acoustic impedance depends on parameters other than bulk modulus.

Based on the concept of an acoustic transmission line, we substitute the abovementioned material parameters
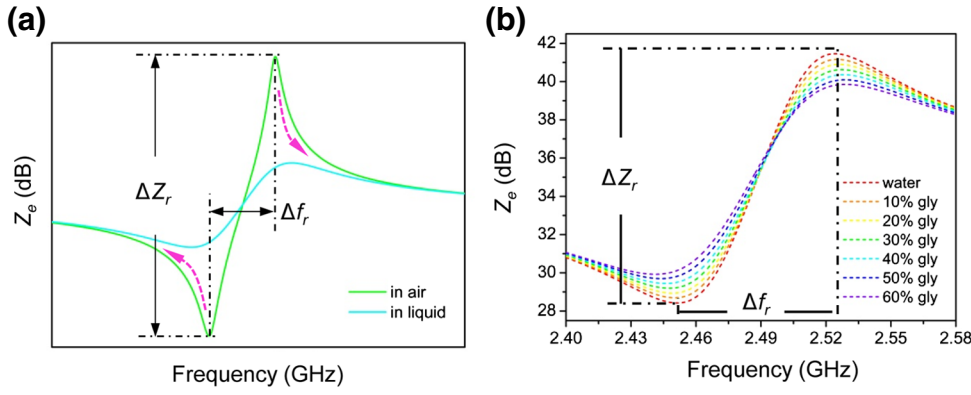
FIG. 4. (a) The simulated Z_e-f curves of the microsensor in (a) air and liquid and (b) the response results of the microsensor loaded with different weight ratios of glycerol-water mixtures. Unit conversion: Z_e (dB) = 20logZ_e (Ohm).

(density, bulk modulus, viscosity, thickness) of the LAWs microsensor and liquid sample. The curves of electrical impedance with frequency (Z_e-f) of the microsensor in air and water are obtained by the software Advanced Design System (ADS). As shown in Fig. 4(a), the difference in the resonant peak, ΔZ_r ($\Delta Z_r = Z_p$-Z_s), representing the acoustic energy stored in the LAW microsensor, would be lost in the liquid as analyzed above, which naturally increases the resonant frequency difference Δf_r ($\Delta f_r = f_p f_s$), as indicated by the pink arrow. In particular, the change trend of the Z_e-f curves between different liquid samples still follows this direction with increasing bulk modulus. For demonstrating the theory, glycerol-water mixtures of different bulk modulus are chosen as the analytical samples. The viscosity, density, and acoustic velocity of samples are measured by commercial instruments at $20\,°C$, with an accuracy of $\pm 0.1\,°C$, and the detailed results are listed in Table I. These values (viscosity, density, and acoustic velocity) agree well with the literature [51,52]. For simple Newtonian fluids (i.e., $|M^*| \approx K'$), the bulk modulus is approximately calculated by [47]

$$K' = \rho v^2. \tag{10}$$

These data also indicate that the acoustic impedance increases with concentration. We substitute these parameters (density, viscosity, and acoustic velocity) of each glycerol-water mixture into the top parallel-liquid stack of the transmission line model sequentially to determine the electrical impedance response of each of them, as shown

in Fig. 4(b). The seven liquid samples show distinct differences due to the differences in bulk modulus whose trend is consistent with the direction of the pink arrow in Fig. 4(a).

IV. EXPERIMENTAL PART

To build a substantial testing platform, a three-dimensional (3D) printing holder is used to fix the assembled sensor-microchannel device, with part of the pads uncovered for probe connecting, as shown in Fig. 5(a). These prepared glycerol-water mixtures are pumped into the microchannel and onto the microsensor at a speed of 10 μl/min. Measurements are performed online by the probe-test set up. It should be noted that the Doppler effect of acoustic waves can be ignored since the flow velocity (0.06 m/s) is much smaller than the acoustic velocity in liquid (approximately 1500 m/s). To ensure measurement accuracy, the microchannel is washed with the test samples for one minute before each sample is tested. In addition, the electrical response of each sample is automatically recorded every second for a total of 30 times through a network analyzer (E8363B, Agilent Technologies) controlled by a MATLAB program to reduce the testing error. The experimental results in Fig. 5(b), which represent one of the 30 records, show good agreement with the simulated results except for the absolute value of the impedance. This discrepancy might derive from fabrication or material defects. More importantly, ΔZ_r and Δf_r are extracted from the 30 records of each sample and both are determined to be linearly correlated with

TABLE I.   Properties of glycerol-water mixtures (at $20\,°C$).

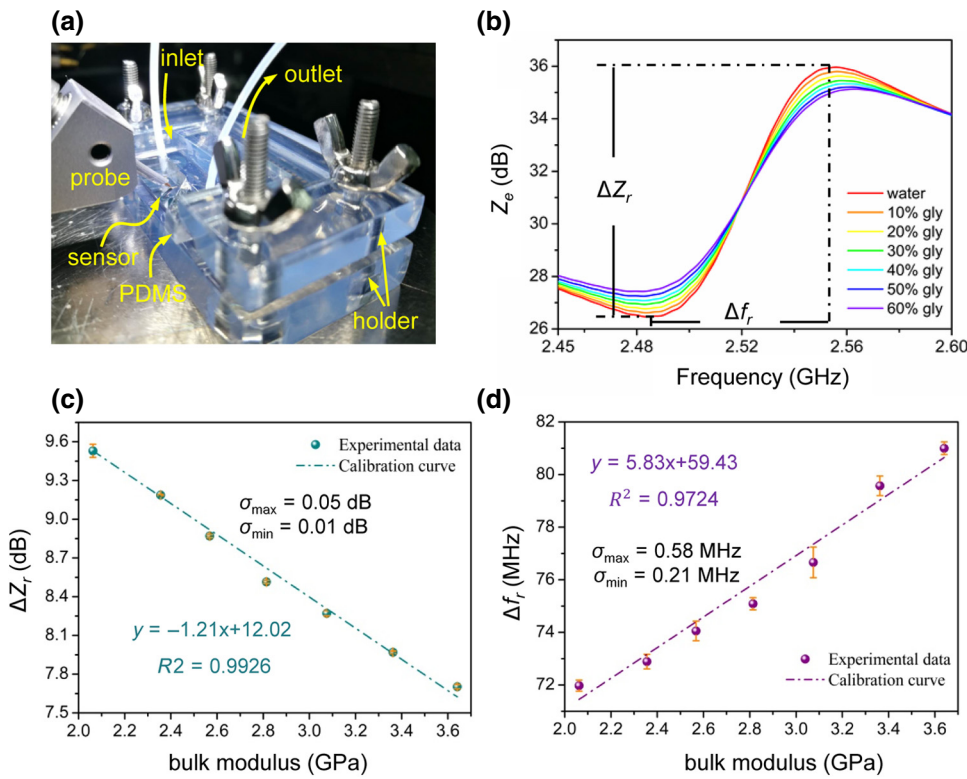| Glycerol (wt. %)	Viscosity η (cP)	Density ρ (g/cm^3)	Acoustic velocity v (m/s)	Bulk modulus K (GPa)
0	0.91	1.002	1462	2.142
10	1.21	1.025	1516	2.355
20	1.62	1.046	1567.2	2.568
30	2.33	1.071	1621.2	2.814
40	3.84	1.096	1675	3.075
50	7.21	1.124	1729.6	3.362
60	11.9	1.148	1780.6	3.640

FIG. 5. (a) Probe-test set up of sensor microchannel fixed by 3D printing holder. (b) Experimental Z_e-f curves of microsensor loaded with glycerol-water mixtures of different bulk modulus. Characteristic curves of (c) ΔZ_r-K and (d) Δf_r-K are drawn by extracted data from (b). All experiments are performed at 20 °C with an accuracy of ± 0.1 °C.

the bulk modulus (K), as shown in Figs. 5(c) and 5(d). Indeed, both parameters demonstrate high linear coefficients ($R^2 = 0.993$, 0.972), indicating a linear relationship between the electrical impedance response and bulk modulus of the loaded liquid. In addition, the maximum standard deviation in the tested $\Delta Z_r - K$ data is 0.05 dB. This finding implies a measurement uncertainty of 0.42 GPa, which can be further improved by minimizing the test uncertainty of $\Delta Z_r - K$. Utilizing these two characteristic curves for calibration, the microsensor is expected to measure the bulk modulus of Newtonian fluids given the density or viscosity of the fluids.

A. Viscosity nonsensitivity validation

As stated in the introduction, the LAWs microsensors should be insensitive to the viscosity of liquids, in contrast to a shear-acoustic-wave sensor. To further demonstrate the reliability of the abovementioned results, that is the nonsensitivity to viscosity of the LAWs microsensors, we vary only the viscosity in the Mason model from 1 to 8 cP, for which the responses of electrical impedance [Fig. 6(a)] are nearly indistinguishable. Furthermore, a noticeable slope gap is observed when comparing the simulation value (ΔZ_r) induced by viscosity and bulk modulus over the same range of values, as shown in the inset of Fig. 6(a). Thus, we can confirm the previous conclusion that the viscosity of liquid sample has very little effect on the acoustic impedances of materials. To obtain further support in the experiments, we carry out viscosity-response testing based

on the physical law that the viscosity of liquids varies significantly with temperature and that changes in the bulk modulus can be ignored. The viscosity of pure glycerol changes by approximately 90% from 40 °C (284 cP) to 80 °C (31.9 cP) [52], while the bulk modulus changes by only 6% (0.28 GPa) [53]; thus, the viscosity is the main parameter that varies during the heating process, and other properties' changes of glycerol-water mixtures can be ignored. The entire device set up with pure glycerol loaded above the microsensor is heated and tested using a temperature-controlled probe table (500 Federal RD. Brookfield, CT.). However, the large changes in viscosity that are induced produce few invisible shifts in ΔZ_r, as indicated by the red curve in Fig. 6(b). The blue curve is a copy of the characteristic curve in Fig. 5(c). These results validate the sensitivity of the longitudinal waves to the bulk modulus and not viscosity. This behavior is completely different from that of shear waves in measuring viscosity.

B. Nanowavelength and nonreflective regime

Although the attenuation of longitudinal waves is inevitable due to the presence of bulk viscosity, the heights of microchannels still need to be designed carefully. On the other hand, longitudinal acoustic waves generated in the microsensor will be reflected to varying degrees at every accessible interface composed of different substances, leading to a disturbance in the main resonance,
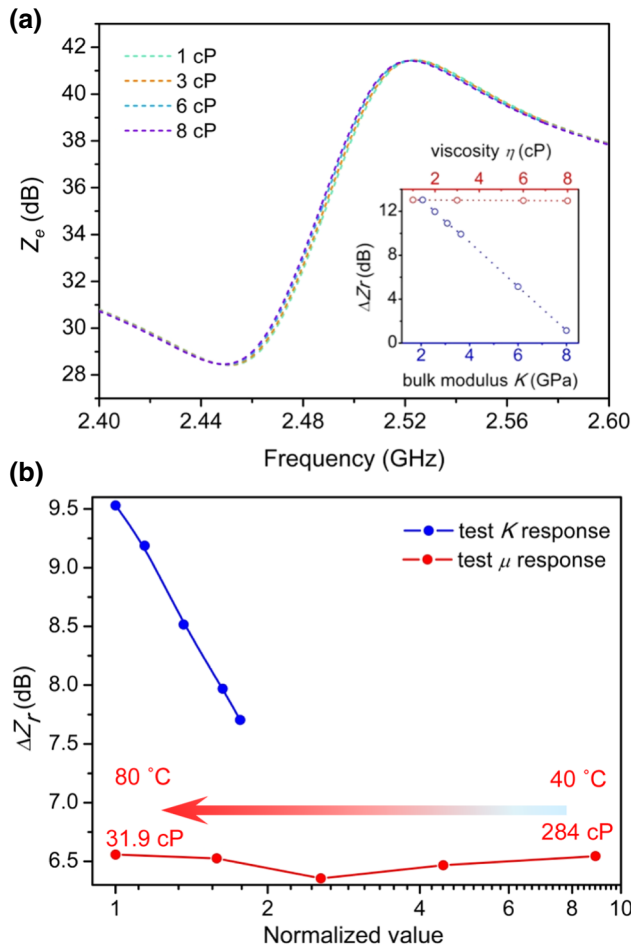
(a)

(b)

FIG. 6. (a) The simulation of electrical impedance corresponding to different viscosity values to prove the nonsensitivity of longitudinal waves to viscosity, inset is the comparison of resonant impedance difference (ΔZ_r) induced by viscosity and bulk modulus. (b) Experimental validation of impedance response of microsensor to viscosity and bulk modulus. All experiments are performed at 20 °C with an accuracy of ±0.1 °C.
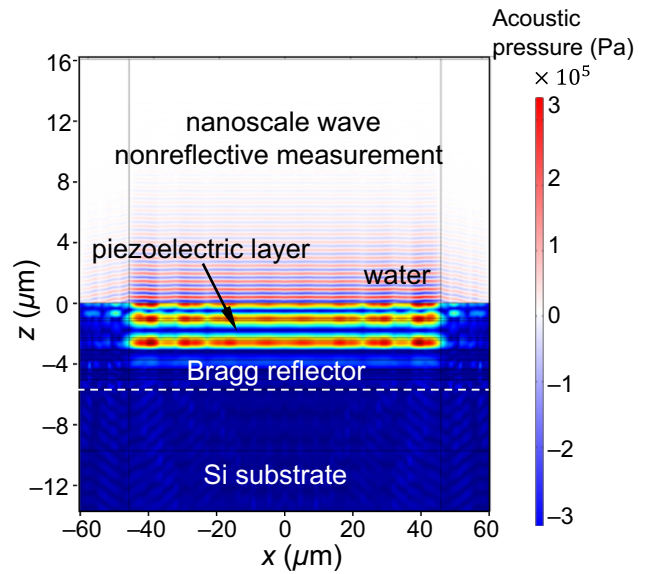

FIG. 7. Two-dimensional FEM simulation of microsensor loaded with 16-μm high water, where the propagation of an approximately 2.5 GHz longitudinal wave forms a nonreflective measurement in micron scales.

which would ultimately affect the validity of the testing. A two-dimensional FEM model is established based on the material and structure of the microsensor in software COMSOL, incorporating modules of solid mechanics (microsensor) and electrostatic and pressure acoustics (water), as illustrated in Fig. 7. To reduce the calculation time, we set the interface of the solid-liquid as a hard sound field boundary (no-slip condition) and the other boundary as an open boundary (slip condition) to simulate a semi-infinite water domain. All material properties used in this model are the default settings of the software. The simulated results indicate that part of the acoustic energy dissipates into water, while the wavelength of 2.5-GHz longitudinal waves is approximately 600 nm, and the nonreflective propagation (approximately 15 μm) occurs in the water domain area (16 μm in height) above the surface of the microsensor. Therefore, smoothed Z_e-f curves,

without reflected acoustic wave interference resonance and related only to the parameters in Eq. (7), are obtained through the tests in the low-height microchannel. The resonant impedance difference ΔZ_r or the resonant frequency difference Δf_r could thus be extracted to establish the corresponding relationship with the bulk modulus. Compared with traditional methods using low-frequency ultrasonic waves, nanoscale acoustic waves can be operated in a thinner layer of liquid with the undeniable advantages of a faster response, high sensitivity, and small size. In addition, the propagation distance of the longitudinal wave in liquids (in water, for instance, the decay length is about 7.7 μm) is much longer than that of a shear wave (in water, for instance, the decay length is about 11 nm) according to their attenuations [30,54]. This indicates that shear waves can be ignored and validates Eq. (7). Consequently, the bulk modulus dominates the electrical response of the LAWs microsensor in a liquid environment.

To study the electrical impedance response under a specific liquid height, we use a Mason model to execute simulation calculations. Figure 8(a) describes the simulated Z_e-f curves of microsensors with a parallel-water stack of different thicknesses. The curves for water layer thicknesses greater than 15 μm are almost exactly the same, which means that the longitudinal wave no longer exists. The inset magnifies the minor differences between the curves. Moreover, resonance with echo interference appears when the thickness of the parallel-water stack is less than or equal to 12 μm. In addition, we fabricate PDMS-based microchannels of different heights (18, 35, 60, and 95 μm) and use them to measure the Z_e-f curves
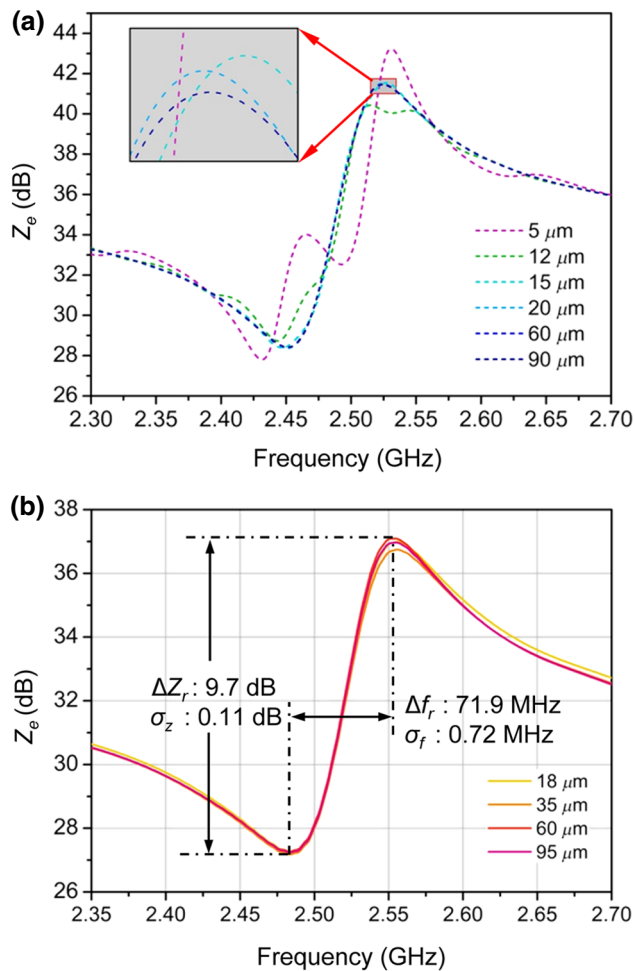
FIG. 8. (a) The simulated Z_e-f curves of the microsensor with parallel-water stacks of different thicknesses by transmission line model showing two kinds of resonance with reflection and no reflection. (b) The measured electrical impedance-frequency response of the microsensor using PDMS-based microchannels of different heights. All experiments are performed at 20 °C with an accuracy of ±0.1 °C.

when pumped with water in microchannels. The measured results [Fig. 8(b)] are similar to those shown in Fig. 8(a) and prove the nonreflective propagation of longitudinal acoustic waves in low-height microchannels. The standard deviations of ΔZ_r and Δf_r among these four curves are 0.11 dB and 0.72 MHz, respectively. Those deviations are slightly greater than those indicated in Figs. 5(c) and 5(d), which might be random errors that arose when superseding microchannels of different heights and can be obviated in fixed-height testing. Finally, we conclude that the measurement of the bulk modulus by GHz LAWs microsensors can be performed for microfluidics of microscale height, which is much smaller than the heights considered suitable for ultrasonic wave detection.

V. CONCLUSION

In this work, we show that the LAWs microsensor is sensitive to the bulk modulus of simple Newtonian liquids based on the interaction of nanowavelength longitudinal acoustic waves and the fluids. The principle is different from that of conventional viscosity measurements performed by shear acoustic waves. The bulk modulus is experimentally acquired in PDMS-based microchannels and agrees well with our theoretical Mason model. A viscosity experiment performed on the LAWs microsensor verifies that it is insensitive to viscosity. Not only does this property give the bulk-modulus sensor a firm footing, it also provides a reliable picture of nanometer longitudinal wave dissipation in liquids. In addition, two-dimensional FEM simulation and nonreflective measurements in microchannels are implemented. Highly sensitive, small, and able to support compact integration and batch fabrication, the LAW microsensor is well suitable for microfluidic applications for disease diagnosis, drug synthesis, medical screening, and other lab-on-chip protocols.

[1] G. A. Urban, Micro- and nanobiosensors—state of the art and trends, Meas. Sci. Technol. **20**, 012001 (2009).

[2] M. Zougagh and Á Ríos, Micro-electromechanical sensors in the analytical field, Analyst **134**, 1274 (2009).

[3] B. Jakoby and M. J. Vellekoop, Physical sensors for liquid properties, IEEE Sens. J. **11**, 3076 (2011).

[4] A. Arbor, W. Stumm, F. M. M. Morel, A. J. Bard, A. Lasaga, M. L. Hitchman, F. C. Anson, F. Zhou, P. R. Unwin, C. Lee, F. Anson, E. R. Scott, H. S. White, B. Phipps, D. H. Craston, and D. Mandler, Chemical microsensors, Science (80-.). **254**, 74 (1990).

[5] P. S. Waggoner and H. G. Craighead, Micro- and nanomechanical sensors for environmental, chemical, and biological detection, Lab Chip **7**, 1238 (2007).

[6] J. Tamayo, P. M. Kosaka, J. J. Ruz, Á San Paulo, and M. Calleja, Biosensors based on nanomechanical systems, Chem. Soc. Rev. **42**, 1287 (2013).

[7] D. J. Beebe, G. A. Mensing, and G. M. Walker, Physics and applications of microfluidics in biology, Annu. Rev. Biomed. Eng. **4**, 261 (2002).

[8] G. M. Whitesides, The origins and the future of microfluidics, Nature **442**, 368 (2006).

[9] I. Dufour, E. Lemaire, B. Caillard, H. Debéda, C. Lucat, S. M. Heinrich, F. Josse, and O. Brand, Effect of

hydrodynamic force on microcantilever vibrations: Applications to liquid-phase chemical sensing, Sens. Actuators B Chem. **192,** 664 (2014).

[10] E. Gil-Santos, C. Baker, D. T. Nguyen, W. Hease, C. Gomez, A. Lemaître, S. Ducci, G. Leo, and I. Favero, High-frequency nano-optomechanical disk resonators in liquids, Nat. Nanotechnol. **10,** 810 (2015).

[11] V. Agache, G. Blanco-Gomez, F. Baleras, and P. Caillat, An embedded microchannel in a MEMS plate resonator for ultrasensitive mass sensing in liquid, Lab Chip **11,** 2598 (2011).

[12] K. Länge, G. Blaess, A. Voigt, R. Götzen, and M. Rapp, Integration of a surface acoustic wave biosensor in a microfluidic polymer chip, Biosens. Bioelectron. **22,** 227 (2006).

[13] G. Luka, A. Ahmadi, H. Najjaran, E. Alocilja, M. Derosa, K. Wolthers, A. Malki, H. Aziz, A. Althani, and M. Hoorfar, Microfluidics integrated biosensors: A leading technology towards lab-on-A-chip and sensing applications, Sensors (Switzerland) **15,** 30011 (2015).

[14] S. A. Pfeiffer and S. Nagl, Microfluidic platforms employing integrated fluorescent or luminescent chemical sensors: A review of methods, scope and applications, Methods Appl. Fluoresc. **3,** 34003 (2015).

[15] V. Yantchev and I. Katardjiev, Thin film Lamb wave resonators in frequency control and sensing applications: A review, J. Micromech. Microeng. **23,** 043001 (2013).

[16] T. Wang, X. Mu, P. Kropelnicki, A. B. Randles, and C. Lee, Viscosity and density decoupling method using a higher order Lamb wave sensor, J. Micromech. Microeng. **24,** 075002 (2014).

[17] K. Länge, B. E. Rapp, and M. Rapp, Surface acoustic wave biosensors: A review, Anal. Bioanal. Chem. **391,** 1509 (2008).

[18] M. Thompson, A. L. Kiplingt, and W. C. Duncan-hewitts, Thickness-shear-mode acoustic wave sensors in the liquid phase. A review, Analyst **116,** 881 (1991).

[19] G. N. M. Ferreira, A. C. da-Silva, and B. Tomé, Acoustic wave biosensors: Physical models and biological applications of quartz crystal microbalance, Trends Biotechnol. **27,** 689 (2009).

[20] Y. Q. Fu, J. K. Luo, N. T. Nguyen, A. J. Walton, A. J. Flewitt, X. T. Zu, Y. Li, G. McHale, A. Matthews, E. Iborra, H. Du, and W. I. Milne, Advances in piezoelectric thin films for acoustic biosensors, acoustofluidics and lab-on-chip applications, Prog. Mater. Sci. **89,** 31 (2017).

[21] Y. Q. Fu, J. K. Luo, X. Y. Du, A. J. Flewitt, Y. Li, G. H. Markx, A. J. Walton, and W. I. Milne, Recent developments on ZnO films for acoustic wave based bio-sensing and microfluidic applications: a review, Sens. Actuators B Chem. **143,** 606 (2010).

[22] G. Wingqvist, J. Bjurström, L. Liljeholm, V. Yantchev, and I. Katardjiev, Shear mode AlN thin film electro-acoustic resonant sensor operation in viscous media, Sens. Actuators B Chem. **123,** 466 (2007).

[23] D. Chen, S. Song, J. Ma, Z. Zhang, P. Wang, W. Liu, and Q. Guo, Micro-electromechanical film bulk acoustic sensor for plasma and whole blood coagulation monitoring, Biosens. Bioelectron. **91,** 465 (2017).

[24] M. Demiguel-Ramos, B. Díaz-Durán, J.-M. Escolano, M. Barba, T. Mirea, J. Olivares, M. Clement, and E. Iborra, Gravimetric biosensor based on a 1.3 GHz AlN shear-mode solidly mounted resonator, Sens. Actuators B Chem. **239,** 1282 (2017).

[25] M. Link, J. Weber, M. Schreiter, W. Wersing, O. Elmazria, and P. Alnot, Sensing characteristics of high-frequency shear mode resonators in glycerol solutions, Sens. Actuators B Chem. **121,** 372 (2007).

[26] H. Qu, Y. Yang, Y. Chang, Z. Tang, W. Pang, Y. Wang, H. Zhang, and X. Duan, On-chip integrated multiple micro-electromechanical resonators to enable the local heating, mixing and viscosity sensing for chemical reactions in a droplet, Sens. Actuators B Chem. **248,** 280 (2017).

[27] F. Liu, A. N. Nordin, F. Li, and I. Voiculescu, A lab-on-chip cell-based biosensor for label-free sensing of water toxicants, Lab Chip **14,** 1270 (2014).

[28] K. Kustanovich, V. Yantchev, V. Kirejev, G. D. M. Jeffries, T. Lobovkina, and A. Jesorka, A high-performance lab-on-a-chip liquid sensor employing surface acoustic wave resonance, J. Micromech. Microeng. **27,** 114002 (2017).

[29] Y. Hongbin, L. Liang, and A. G. Yuandong, Capacitive micromachined ultrasonic transducer (CMUT) based micro viscosity sensor, Sens. Actuators B Chem. **227,** 346 (2016).

[30] K. K. Kanazawa and J. G. Gordon, The oscillation frequency of a quartz resonator in contact with liquid, Anal. Chim. Acta **175,** 99 (1985).

[31] W. C. Duncan-Hewitt, M. Thompson, and M. Thompson, Four-layer theory for the acoustic shear wave sensor in liquids incorporating interfacial slip and liquid structure, Anal. Chem. **64,** 94 (1992).

[32] G. G. Stokes, On the theories of the internal friction of fluids in motion, and of the equilibrium and motion of elastic solids, Trans. Camb. Philos. Soc. **8,** 75 (1845).

[33] A. Teplykh, B. Zaitsev, and I. Kuznetsova, in IEEE Int. Ultrason. Symp. IUS 1049 (2013).

[34] V. C. Mow, M. H. Holmes, and W. Michael Lai, Fluid transport and mechanical properties of articular cartilage: A review, J. Biomech. **17,** 377 (1984).

[35] Y. C. Fung, *BiomechanicsâĂŕ: Mechanical Properties of Living Tissues* (Springer Science & Business Media, New York, 2013).

[36] G. W. Kim and K. W. Wang, On-line estimation of effective bulk modulus in fluid power systems using piezoelectric transducer impedance, J. Intell. Mater. Syst. Struct. **20,** 2101 (2009).

[37] C. Niezrecki, J. K. Schueller, and K. Balasubramanian, Piezoelectric-based fluid bulk modulus sensor, J. Intell. Mater. Syst. Struct. **15,** 893 (2004).

[38] H. Antlinger, S. Clara, R. Beigelbeck, S. Cerimovic, F. Keplinger, and B. Jakoby, Sensing the characteristic acoustic impedance of a fluid utilizing acoustic pressure waves, Sens. Actuators A Phys. **186,** 94 (2012).

[39] X. Wencheng, Z. Xu, S. Choi, and C. Junseok, A high-quality-factor film bulk acoustic resonator in liquid for biosensing applications, Microelectromech. Syst. J. **20,** 213 (2011).

[40] J. Liang, Z. Liu, H. Zhang, B. Liu, M. Zhang, H. Zhang, and W. Pang, On-chip nanofluidic integration of acoustic

sensors towards high Q in liquid, Appl. Phys. Lett. **111,** 1 (2017).

[41] Y. Lu, H. Zhang, Y. Jiang, H. Zhang, W. Pang, and M. Zhang, in 2018 IEEE Micro Electro Mech. Syst. 854 (2018).

[42] Y. Zhang, J. Luo, A. J. Flewitt, Z. Cai, and X. Zhao, Film bulk acoustic resonators (FBARs) as biosensors: A review, Biosens. Bioelectron. **116,** 1 (2018).

[43] C. Verdier, P. Y. Longin, and M. Piau, Dynamic shear and compressional behavior of polydimethylsiloxanes: Ultrasonic and low frequency characterization, Rheol. Acta **37,** 234 (1998).

[44] W. M. Slie, A. R. Donfor, and T. A. Litovitz, Ultrasonic shear and longitudinal measurements in aqueous glycerol, J. Chem. Phys. **44,** 3712 (1966).

[45] K. M. Lakin, G. R. Kline, and K. T. McCarron, High-Q microwave acoustic resonators and filters, IEEE Trans. Microw. Theory Tech. **41,** 2139 (1993).

[46] B. A. Auld, *Acoustic Fields and Waves in Solids* (Willey, New York, 1973).

[47] C. Verdier and M. Piau, Acoustic wave propagation in two-phase viscoelastic fluids: The case of polymer emulsions, J. Acoust. Soc. Am. **101,** 1868 (1997).

[48] C. Prugne, J. Van Est, B. Cros, G. Lévêque, and J. Attal, Measurement of the viscosity of liquids by near-field acoustics, Meas. Sci. Technol. **9,** 1894 (1998).

[49] P. Y. Longin, C. Verdier, and M. Piau, Dynamic shear rheology of high molecular weight polydimethylsiloxanes: comparison of rheometry and ultrasound, J. Nonnewton. Fluid Mech. **76,** 213 (1998).

[50] J. Holmes, G. Parker, and W. Povey, Temperature dependence of bulk viscosity in water using acoustic spectroscopy, J. Phys. Conf. Ser. **269,** 012011 (2011).

[51] K. Takamura, H. Fischer, and N. R. Morrow, Physical properties of aqueous glycerol solutions, J. Pet. Sci. Eng. **98–99,** 50 (2012).

[52] J. B. Segur and H. E. Oberstar, Viscosity of glycerol and its aqueous solutions, Ind. Eng. Chem. **43,** 2117 (1951).

[53] R. Payri, F. J. Salvador, J. Gimeno, and G. Bracho, The effect of temperature and pressure on thermodynamic properties of diesel and biodiesel fuels, Fuel **90,** 1172 (2011).

[54] A. S. Dukhin and P. J. Goetz, Bulk viscosity and compressibility measurement using acoustic spectroscopy, J. Chem. Phys. **130,** 124519 (2009).